Journal Pre-proof

The mimetic assembly of cobalt prot-porphyrin with cyclodextrin dimer and its application for H_2O_2 detection

Miao-Feng Fan, Hui-Min Wang, Li-Jiao Nan, Ai-Jun Wang, Xiliang Luo, Pei-Xin Yuan, Jiu-Ju Feng

PII: S0003-2670(19)31343-1

DOI: https://doi.org/10.1016/j.aca.2019.11.002

Reference: ACA 237212

To appear in: *Analytica Chimica Acta*

Received Date: 18 September 2019

Revised Date: 28 October 2019

Accepted Date: 3 November 2019

Please cite this article as: M.-F. Fan, H.-M. Wang, L.-J. Nan, A.-J. Wang, X. Luo, P.-X. Yuan, J.-J. Feng, The mimetic assembly of cobalt prot-porphyrin with cyclodextrin dimer and its application for H_2O_2 detection, *Analytica Chimica Acta*, https://doi.org/10.1016/j.aca.2019.11.002.

Graphical Abstract

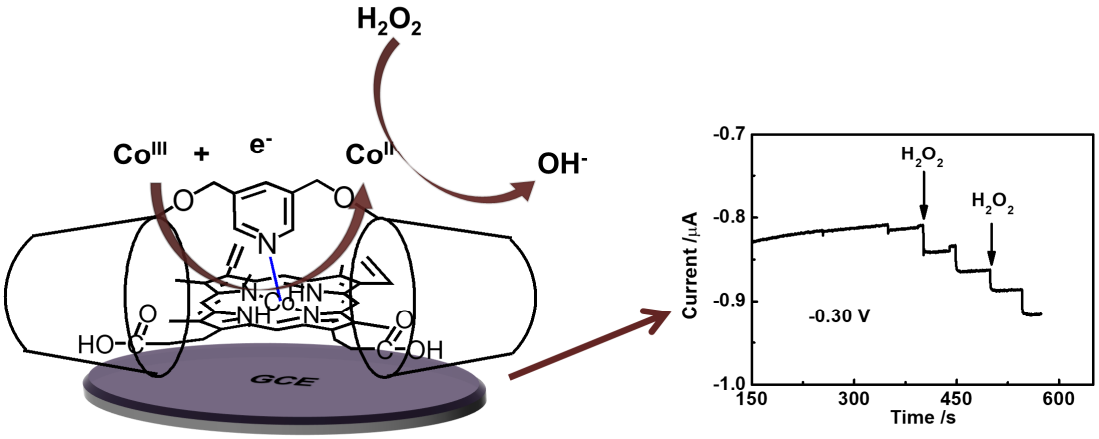

The mimetic assembly of cobalt prot-porphyrin with cyclodextrin dimer and its application for H_2O_2 detection

Miao-Feng Fan,[a] Hui-Min Wang,[a] Li-Jiao Nan,[a] Ai-Jun Wang,[a] Xiliang Luo,[b] Pei-Xin Yuan,[a]* Jiu-Ju Feng [a]*

[a] *Key laboratory of the Ministry of Education for Advanced Catalysis Materials, College of Chemistry and Life Sciences, College of Geography and Environmental Sciences, Zhejiang Normal University, Jinhua 321004, China*

[b] *Key Laboratory of Sensor Analysis of Tumor Marker, Ministry of Education, College of Chemistry and Molecular Engineering, Qingdao University of Science and Technology, Qingdao 266042, China*

**Corresponding author: ypxdr@zjnu.edu.cn (P.X. Yuan); jjfeng@zjnu.cn (J.J. Feng).*

Abstract

A biomimetic assembly of per-O-methylated-cyclodextrin dimer with cobalt proto-porphyrin (Co^{III}-PPIX@Py2CD) was achieved via covalent linkage between Co^{III} of Co^{III}-PPIX and pyridine N of Py2CD (primarily synthesized by the acyl chlorination reaction of two β-CDs monomers with 3,5-bis (bromomethyl) pyridine). Ultraviolet-visible (UV-vis) and circular dichroism (CD) absorption spectroscopy, and NMR hydrogen spectroscopy (H^1-NMR) were adopted to carefully characterize the structure of Py2CD and its functional assembly with Co^{III}-PPIX. X-ray photoelectron spectroscopy (XPS) was employed to affirm the binding of the as-obtained Co^{III}-PPIX@Py2CD, whose electrochemical kinetics were extensively studied to validate the feasibility in the catalytic reduction of hydrogen peroxide (H_2O_2). The developed sensor displayed the wide linear range for H_2O_2 detection and the low detection limit of 2.47×10^{-7} M. This work sheds some constructive lights on rational design and synthesis of preeminently biomimic carrier and high cost-effectiveness catalyst for (bio)analytical applications.

Keywords: β-cyclodextrin; Porphyrin; Mimetic assembly; Biosensor

1. Introduction

Nowadays, ultrasensitive and highly selective determination of hydrogen peroxide (H_2O_2) is imperative in environmental monitoring, pharmacokinetics research and biomedical engineering [1-3]. For that, many biosensors were developed based on unprecedentedly electrocatalytic property of conventional enzymes such as cytochrome c oxidase and horseradish peroxidase (HRP) [3, 4]. However, the high price and critical preservation/application conditions for natural enzymes seriously hinder their applications in practice [5].

As a cofactor of enzyme, porphyrin with macrocyclic conjugated organic molecules has drawn extensive attention in electrocatalysis towards reduction or oxidation of small molecules [6, 7]. Especially, cobalt ion chelated with porphyrin ring to form stable complex, plays a key role in electron transfer, energy conversion, and nonlinear optical-limiting under specifically physiological processes [8, 9]. Therefore, it would be feasible to simulate the structure and activity of natural enzyme by functional assembly of porphyrin with other matrices.

As we know, one-dimensional advanced nanomaterials such as graphene [10] and carbon nanotubes [11] were introduced as artificial frameworks to load porphyrin by covalent or non-covalent methods. These hybrid nanocomposites can effectively avoid the structure destruction and aggregation of porphyrin, and enhance the catalytic activity and stability of the supported porphyrin with regard to the monomer itself. For example, *G*-quadruplex DNA sequences associated with porphyrin [12] displayed the comparable catalytic characters relative to natural HRP in bioassays.

Nevertheless, the catalytic activity is very lower to meet the requirement in ultrasensitive analysis by replacing *G*-quadruplex DNA sequences with Co ion, owing to their non-axial bond with pyridine to form enzyme-like five-coordinated structures [13].

Cyclodextrin (CD) as a class of cyclic oligosaccharides containing 6, 7, or 8 glucose units (named α-, β-, or γ-CD, respectively), displays the toroidal structure in a hydrophobic inner cavity and a hydrophilic exterior [14-16]. In general, β-CD is an ideal host-guest carrier to adopt various small molecules such as porphyrin into their hydrophobic cavities [17, 18], albeit with their noticeable reduction in the catalytic activity and the steady of the included guests [17, 19].

Inspired by the natural configuration of vitamin B12, two β-CD monomers were linked with 3,5-bis (bromomethyl) pyridine to form per-O-methylated-cyclodextrin dimer (Py2CD), which would be ideal support for functional assembly [20]. By virtue of this carrier, Co^{III} can effectively bind with the pyridine N of Py2CD in an axial coordinate and the porphyrin ring is encysted with β-CD to stabilize the structure of porphyrin monomer. Besides, 3,5-bis (bromomethyl) pyridine enables the exposure of more active sites of cobalt proto-porphyrin (Co^{III}-PPIX) into the aqueous solution, which has strong affinity to oxygenated substances (e.g. O_2 and H_2O_2).

In this work, simulating the structure of VB_{12}, Py2CD was synthesized by the covalent linkage of two β-CDs monomers with 3,5-bis (bromomethyl) pyridine, which was further combined with Co^{III}-PPIX via the coordination of Co^{III} and pyridine N to form the biomimetic catalyzer (defined as Co^{III}-PPIX@Py2CD for

clarity). The electrocatalytic activity and electron transfer of the hybrid nanocomposite were investigated in details, followed by exploring their feasibility for electrochemical detection of H_2O_2 in this research (Scheme 1).

2. Experimental section

2.1. Reagents and materials

Typically, β-CD, sodium hydride (NaH), trichloromethane ($CHCl_3$), sodium bicarbonate ($NaHCO_3$), dimethyl sulfoxide (DMSO), H_2O_2, hydrogen chloride (HCl), dimethyl formamide (DMF), *N*-hydroxysuccinimide (NHS), 3,5-bis (bromomethyl) pyridine, deuterated chloroform ($CDCl_3$), iron trichloride ($FeCl_3$), potassium persulfate ($K_2S_2O_8$), potassium permanganate ($KMnO_4$), ascorbic acid (AA) and dopamine (DA) were purchased from Shanghai Aladdin Chemical Reagent Company (Shanghai, China). Co^{III}-PPIX was received from J&K Scientific Ltd (Shanghai, China).

Besides, 0.1 M phosphate buffer solution (PBS) with different pH was prepared by mixing 0.1 M KH_2PO_4, 0.1 M K_2HPO_4 and 0.1 M KNO_3 stock solutions together, which is behaved as the supporting electrolyte. The O_2- or N_2-saturated electrolyte was firstly bubbled with high-purity O_2 or N_2 for 30 min and then preserved the atmospheric pressure during the whole test. Ultrapure water was obtained from a Millipore water purification system (≥18 MΩ, Milli-Q, Millipore), and implemented throughout all the assays.

2.2. Characterization

The circular dichroism (CD) spectra of the samples were acquired with a Jasco J-810/163-900 circular dichroism chiroptical spectrometer at 25 °C. Ultraviolet-visible (UV-vis) absorption spectra were recorded with the Thermo nicolet evolution 500 UV-vis spectrometer (Beijing Puxi general instrument Co., Ltd., China) in the wavelength region of 200-800 nm. NMR hydrogen spectroscopy (H^1-NMR) measurements were conducted with a Bruker AMX-500 spectrometer at 600 MHz, by employing tetramethylsilane (TMS) as the reference and $CDCl_3$ as the solvent.

Electrochemical experiments were performed on a CHI 660D electrochemical workstation (Shanghai Chenghua Instruments Inc., China) with a conventional three-electrode system, where a glassy carbon electrode (GCE, 3 mm in diameter) performed as the working electrode, a saturated calomel electrode (SCE) as the reference electrode and a platinum wire as the counter electrode.

2.3. Synthesis of Py2CD

For typical synthesis of Py2CD, the fabrication and separation procedures were almost identical to those previously published in the literature [21, 22]. First, the dried β-CD (7.1 g, 6.3 mmol) was dissolved into dry DMSO (40 mL) by continuously stirring for 2 h at 55 °C under the N_2-saturated atmosphere. Then, NaH oiliness solution was put into the mixed solution slowly (where the ratio of the β-CD:NaH remained 5:1) under stirring for 2 h to obtain a homogeneous solution. Then, 3, 5-bis(bromomethyl) pyridine hydrobromide (1.0 g, 2.9 mmol) was introduced into the

reaction system and stirred overnight. Next, the mixture was neutralized with the diluted aqueous HCl solution (1 M), followed by harvesting the rude Py2CD.

To gain the Py2CD with high purity, the as-prepared product was immersed into methanol gradually to eliminate superfluous NaH under the ice-bath conditions until the solution became transparent. The after-reaction solution was vacuumed and distillated to get rid of the organic solvent. The remainder powder was dissolved into the $NaHCO_3$ solution (0.1 M) and purified by silica gel column chromatography with the fixed ratio of chloroform to methanol (10:1), ultimately drying the purified Py2CD prior to use.

2.4. The synthesis of Co^{III}-PPIX@Py2CD complex

The Co^{III}-PPIX@Py2CD nanocomposite was prepared according to the adsorption and chelation interactions [23, 24]. In brief, the Co^{III}-PPIX/DMF solution (5 μM, 1 mL) was dropwise put into 1 mL of the as-obtained Py2CD aqueous suspension (0.25 mg mL^{-1}) under vigorous stirring. The system was kept reacting for 2 h, accompanied by filtrating to remove the excess Co^{III}-PPIX. The precipitation was dried in a vacuum at 60 °C overnight for further characterization and use.

2.5. The Co^{III}-PPIX@Py2CD modified the electrode

Prior to the electrochemical measurements, the GCE was cleaned firstly by polishing with 0.3 and 0.05 μm aluminum slurry sequentially, and then rinsed thoroughly with water to remove the residual alumina powder. Meanwhile, 0.2 mg of

the Co^{III}-PPIX@Py2CD was well dispersed into 1 mL of water through ultrasonication for 30 min to obtain a homogeneous suspension. Next, 1 mL of the suspension was casted onto the freshly-polished electrode surface and dried in air at room temperature. For comparison, Co^{III}-PPIX modified electrode was prepared by the same method in the controlled experiments.

3. Results and discussion

3.1. The UV-vis and CD characterization

For the structure and stability of the Co^{III}-PPIX@Py2CD complexes, a series of CD and UV-vis absorption spectra were acquired to verify the formation of the nanocomposite. As Fig. 1A depicts, a couple of strong positive/negative absorbance peaks appears at 417/410 nm in the CD spectrum of Co^{III}-PPIX (curve a), respectively, due to the unsymmetrical structure of Co^{III}-PPIX. However, nearly no CD absorption detected in the visible region, while the typical bands of epoxide show up at 248 and 282 nm, corresponding to the right-handed β-helix (curve b) [25, 26]. After the Co^{III}-PPIX has been riveted into the burrow of Py2CD, a pair of absorbance peaks emerges at 468/425 nm, displaying the positive shifts (about 41/15 nm) alternative to those of Co^{III}-PPIX, coupled with the emergence of the weak right-handed β-helix absorption peaks at 257 nm and 286 nm (curve c). These scenarios demonstrate the efficient conjugation between Co^{III}-PPIX and Py2CD in this synthesis.

Fig. 1B shows the UV-vis absorption spectra to corroborate the structure and the adhesion of Py2CD with Co^{III}-PPIX. There is an obvious Soret band appeared at 420

nm (curve a), which is originated from pure porphyrin [27]. Meanwhile, the Q bands located at 529 and 564 nm correspond to the asymmetric plane of porphyrin in Co^{III}-PPIX [28]. After the combination of Co^{III}-PPIX and Py2CD, the Soret band is red-shifted slightly from 420 to 424 nm, and the Q bands display the red shifts from 529/564 nm to 535/568 nm (curve b), respectively. Therefore, the distinct changes in the UV-vis absorption spectra confirm the formation of the Co^{III}-PPIX@Py2CD via the axial coordination between pyridine N of Py2CD and Co^{III} of Co^{III}-PPIX [29].

3.2. The interactions of Py2CD with Co^{III}-PPIX

For this strategy, the ^1H NMR spectrum was recorded to characterize the synthesis of Py2CD adduct in $CDCl_3$ solution. As shown in Fig. 2A, seven singlet proton signals emerge at 0.208, 1.372, 2.059, 2.558, 3.154, 3.190, and 3.891 ppm for the OCH_3 protons framework, which are well assigned to the O-methyl groups of Py2CD at the 2- and 3-positions [30], in good agreement with those detected by the ^1H-detected multiband heteronuclear multiple quantum coherence spectrum (where certifies the emergence of a six-coordinate diamagnetic complex). It means the efficient linkage of the pyridine ligand in the Py2CD coordinates [31].

X-ray photoelectron spectroscopy (XPS) can be widely used to characterize species and valence states of the surface elements [32, 33]. Herein, XPS analysis was performed to carefully examine the combination between Py2CD with Co^{III}-PPIX. As Fig. 2B describes, an obvious XPS peak is located at the binding energy of 398.4 eV for the Py2CD in the high-resolution N 1s XPS spectrum (curve a), belonging to the

pyridinic N in this study [34]. After the effective interactions of the pyridinic N with Co^{III}-PPIX, the XPS peak at 398.4 eV negatively shifts to 397.8 eV (curve b), owing to the stable assembly of pyridinic N with Co^{III} [6].

Meanwhile, the high-resolution Co 2p XPS segments of Co^{III}-PPIX and Co^{III}-PPIX@Py2CD were provided to illuminate the bond information of the assembly. As illustrated in Fig. 2C, the dual XPS peaks appear at 781.0 and 795.4 eV in the high-resolution Co 2p XPS pattern of Co^{III}-PPIX (curve a) , which are ascribed to Co $2p_{3/2}$ and Co $2p_{1/2}$ in the porphyrin [35]. When the axial assembly of Co^{III}-PPIX with Py2CD, the Co $2p_{3/2}$ and Co $2p_{1/2}$ peaks have the positive shifts to 782.3 and 796.0 eV (curve b), thanks to the directional affinity of Co to N with the dramatically enhanced local electronegativity [36, 37]. Hence, the Co^{III}-PPIX@Py2CD is formed *via* the efficient association of Co^{III}-PPIX with Py2CD, where pyridinic N behaves as the linker.

3.3. The electrocatalytic kinetics of Co^{III}-PPIX@Py2CD

The catalytic property of the Co^{III}-PPIX@Py2CD for oxygen reduction reaction (ORR) is a key parameter in this research [38]. Fig. 3A displays the cyclic voltammetry (CV) curves of Co^{III}-PPIX and Co^{III}-PPIX@Py2CD in the air-saturated PBS. Specially, an obvious reduction peak shows up at -0.35 V for Co^{III}-PPIX (curve a), while this peak is positively shifted to -0.26 V in the case of Co^{III}-PPIX@Py2CD (curve b), reflecting the faster electron transfer occurred at the Co^{III}-PPIX@Py2CD. Moreover, the presence of 10 mM H_2O_2 enables the dramatic increase in the reduction

peak current, albeit with negligible impact on the peak position, confirming the feasibility of the as-developed biosensor (curve c).

For the Co^{III}-PPIX (Fig. 3B, curve a), an obvious reduction peak is observed at -0.35 V (E_{pc}) and a small oxidation peak is located at -0.25 V (E_{pa}) in the N_2-saturated circumstance (Fig. 3B, curve a), corresponding to the reduction and oxidation of Co^{III} and Co^{II} species [39], respectively. Besides, the difference between the E_{pa} and E_{pc} (i.e. ΔE_p) is roughly 100 mV. More notably, the more well-defined redox peaks of the Co^{III}-PPIX@Py2CD (Fig. 3B, curve b) appear at -0.26 and -0.18 V with a smaller ΔE_p (79 mV) for the Co^{3+}/Co^{2+} transformation, showing the distinctly enhanced electron transfer in the presence of Py2CD. . Meanwhile, the overpotential of the E_{pc} is decreased with a value of 27 mV for the Co^{III}-PPIX@Py2CD when compared with that of the Co^{III}-PPIX, illustrating the slight increase in the located electron density for the resultant complex.

Insets in Fig. 3B provide the plots of the cathodic peak current (i_{pc}) versus (*vs.*) the scan rate (v) at the Co^{III}-PPIX and Co^{III}-PPIX@Py2CD, where the i_{pc} is proportional to the enlarged scan rate, suggesting that the ORR follows the surface-controlled process [40]. For the Co^{III}-PPIX@Py2CD, the linear equations of the cathodic peak current (i_{pc}) and anodic peak current (i_{pa}) are described as $i_{pc} = -4.85 \times 10^{-8}\nu - 1.073 \times 10^{-6}$ ($R^2 = 0.992$, line b1) and $i_{pa} = 1.97 \times 10^{-8}\nu - 1.21 \times 10^{-7}$ with the correlation coefficient (R^2) of 0.990. Alternatively, for the Co^{III}-PPIX, the linear equations are described as $i_{pc} = -3.73 \times 10^{-8}\nu - 1.004 \times 10^{-6}$ ($R^2 = 0.990$, line a1), and $i_{pa} = 1.85 \times 10^{-8}\nu - 6.60 \times 10^{-9}$ ($R^2 = 0.993$) (data not shown).

The charge-transfer coefficient (α) can be calculated based on the equation: $\alpha = |i_{pc}|/(|i_{pc}| + |i_{pa}|)$, and finds that the α values are roughly 0.63 and 0.73 for Co^{III}-PPIX@Py2CD and Co^{III}-PPIX, respectively. By comparison, the reversibility of the Co^{III}-PPIX@Py2CD is surpassed that of Co^{III}-PPIX under such conditions. Besides, the ΔE_p is close to 59/*z* mV (*z* is the charge-transfer number at 293 K) for Co^{III}-PPIX@Py2CD alternative to that of Co^{III}-PPIX based on the Nernstian equation, so the electronic reaction is illustrated as equation 1:

$$Co^{III}\text{-PPIX} + e^- \rightarrow Co^{II}\text{-PPIX} \quad [1]$$

Hence, with the axial assembly between Py2CD and Co^{III}-PPIX, the Co^{III}-PPIX@Py2CD would not only effectively enhance the electrocatalysis, but also stabilize the in-situ generated intermediates from Co^{III}-PPIX, owing to the enhanced density of the valency electrons in this context. Also, the electrocatalysis of oxygen reduction at the Co^{III}-PPIX@Py2CD is much superior than other matrices such as N-doped nanocomposites and polymers [41, 42], which certifies the special flexibility to stabilize the porphyrin ring for enhancing the affinity of oxygen molecular with metal ion.

The pH influences on the electrocatalytic kinetics of Co^{III}-PPIX@Py2CD were carefully examined by CV in the pH scope of 5.0 ~ 9.0. Fig. 3C shows the positive shifts of the E_{pc} with the boosted pH, which can be described as E_{pc} = -0.0538 + 0.034pH (correlation coefficient R^2 = 0.990, inset in Fig. 3C). Specifically, the protons reaction coincides well with the theory equation of $E^{\Theta'} = K + (mRT/nF)\ln[H^+] = K - 0.058mpH$ (293 K, n = 1/2). It is explained by the fact that the

Co^{III}-PPIX@Py2CD can effectively catalyze the initial reduction of O_2 to H_2O_2 and then further transformed into H_2O, as described below (equations 2~3) [43]:

$$Co^{III}\text{-PPIX@Py2CD} + e^- \rightarrow Co^{II}\text{-PPIX@Py2CD} \quad [2]$$

$$Co^{II}\text{-PPIX@Py2CD} + (1/2)\ H_2O_2 \rightarrow Co^{III}\text{-PPIX@Py2CD} + OH^- \quad [3]$$

3.4. The chronoamperometric detection of H_2O_2 with Co^{III}-PPIX@Py2CD

By virtue of the largely enhanced electrocatalytic features of the Co^{III}-PPIX@Py2CD towards H_2O_2 reduction, an ultrasensitive biosensor for H_2O_2 detection was constructed. The steady-state chronoamperometric curve was recorded by the successive addition of H_2O_2 at the applied potential of -0.30 V (Fig. 4A). To ensure the reliability and stability of the detection signals, the response time of every concentration point was less than 10 s until the steady-state current was obtained.

As expected, the reduction peak current increases with the elevated H_2O_2 concentration, and shows a linear relationship in the range of 10^{-4}~10^{-6} M (R = 0.990, Fig. 4B). The linear regression equation is depicted as $\Delta i = 1.9\times10^{-9}c + 5.693\times10^{-7}$, where Δi refers to the change in the current and c is the H_2O_2 concentration. Also, the detection limit (LOD) is down to 2.47×10^{-7} M (S/N = 3) based on the 3σ method, which reflects the more sensitivity than those of the other referenced platforms (Table 1). It means the highly boosted catalytic characters of Co^{III}-PPIX@Py2CD in this system.

The currents of the interferences were acquired to validate the steady of the detection platform. As described in Fig. 4C, there is no any obvious disturbance

associated with the currents detected (less than 0.6%) in the detection system for reductive interfering substances (e.g. AA and DA), coupled with the distinctly shortened response time. It shows the high tolerability of the reductive interferences for the developed platform.

Besides, the oxidative interferences such as Fe^{3+}, MnO_4^- and $K_2S_2O_8$ are also introduced into the detection system. Fig. 4D shows the respective amperometric curves. There are negligible signals detected (less than 1.2%) after the injection of the interfering substances, clearly indicating that these interferences have slight effects on the assay of H_2O_2 at the same potential. It reveals the high selectivity of the Co^{III}-PPIX@Py2CD in this strategy.

4. Conclusions

In summary, the Co^{III}-PPIX@Py2CD with high catalytic efficiency was synthesized via the axial coordination, using Co^{III}-PPIX as guest molecule and Py2CD with pyridine linker as the carrier. The CD absorption spectra, UV-vis absorption and ^1H NMR spectra confirmed the covalent bond of Co^{III}-PPIX with Py2CD in the specific proportion. Then, the CV experiments demonstrated the facilitated electron transfer rate (about 1.3 times) and the smaller overpotential (with the decay of about 27 mV) when compared to those of single Co^{III}-PPIX under the identical conditions. Moreover, the catalytic process of Co^{III}-PPIX@Py2CD for H_2O_2 reduction followed proton transfer equation and fast reaction rate, showing the distinctly enhanced reduction activity (about 1.25 times) relative to that of Co^{III}-PPIX, as well as the

improved stability against the degradation of the cofactors. Under the optimal conditions, the catalytic currents of the Co^{III}-PPIX@Py2CD exhibited the linear relationship with the H_2O_2 concentrations from 10^{-4} to 10^{-6} M, with the LOD of 2.47 $\times 10^{-7}$ M, along with the high sensitivity and strong anti-interfering ability towards both oxidative and reductive species. Hence, the current strategy offers some valuable guidelines for porphyrin-based biomimetic assembly and the construction of nonenzymatic biosensors.

Acknowledgment

This research was supported by National Natural Science Foundation of China (No.21475118 and 21675093), Basic Public Welfare Research Project of Zhejiang Province (No. LGG18E010001 and GG19B050003), National Natural Science Foundation of Zhejiang Province (No. Q19B050016), Foundation of Key Laboratory of Sensor Analysis of Tumor Marker, Ministry of Education, Qingdao University of Science and Technology (No. SATM201703, STAM201804), the Open Research Fund of Key Laboratory of the Ministry of Education for Advanced Catalysis Materials (Zhejiang Normal University).

References

[1] T.I. Kim, B. Hwang, B. Lee, J. Bae, Y. Kim, Selective monitoring and imaging of eosinophil peroxidase activity with a j-aggregating probe, J. Am. Chem. Soc. 140(37) (2018) 11771-11776.

[2] M.A. Komkova, E.E. Karyakina, A.A. Karyakin, Catalytically synthesized prussian blue nanoparticles defeating natural enzyme peroxidase, J. Am. Chem. Soc. 140(36) (2018) 11302-11307.

[3] B.B. Hu, F.Y. Dai, Z.M. Fan, G.H. Ma, Q.W. Tang, X. Zhang, Nanotheranostics: Congo red/rutin-MNPs with enhanced magnetic resonance imaging and H_2O_2-responsive therapy of Alzheimer's disease in APPswe/PS1dE9 transgenic mice, Adv. Mater. 27(37) (2015) 5499-5505.

[4] N. Aydemir, H. McArdle, S. Patel, W. Whitford, C.W. Evans, J. Travas Sejdic, D.E. Williams, A label-free, sensitive, real-time, semiquantitative electrochemical measurement method for DNA polymerase amplification (ePCR), Anal. Chem. 87(10) (2015) 5189-5197.

[5] K.F. Aguey Zinsou, P.V. Bernhardt, U. Kappler, A.G. McEwan, Direct electrochemistry of a bacterial sulfite dehydrogenase, J. Am. Chem. Soc. 125(2) (2003) 530-535.

[6] S.Y. Deng, P.X. Yuan, X.B. Ji, D. Shan, X.J. Zhang, Carbon nitride nanosheet-supported porphyrin: a new biomimetic catalyst for highly efficient bioanalysis, ACS Appl. Mat. Inter. 7(1) (2015) 543-552.

[7] X.M. Hu, M.H. Rønne, S.U. Pedersen, T. Skrydstrup, K. Daasbjerg, Enhanced catalytic activity of cobalt porphyrin in CO_2 electroreduction upon immobilization on carbon materials, Angew. Chem. Int. Ed. 56(23) (2017) 6468-6472.

[8] D. Nguyen, G. Kang, N. Chiang, X. Chen, T. Seideman, M.C. Hersam, G.C. Schatz, R.P. Van Duyne, Probing molecular-scale catalytic interactions between oxygen and cobalt phthalocyanine using tip-enhanced raman spectroscopy, J. Am. Chem. Soc. 140(18) (2018) 5948-5954.

[9] Z.L. Dong, L.Z. Feng, Y. Hao, M.C. Chen, M. Gao, Y. Chao, H. Zhao, W.W. Zhu, J.J. Liu, C. Liang, Q. Zhang, Z. Liu, Synthesis of hollow biomineralized $CaCO_3$-polydopamine nanoparticles for multimodal imaging-guided cancer photodynamic therapy with reduced skin photosensitivity, J. Am. Chem. Soc. 140(6) (2018) 2165-2178.

[10] S. Pyo, J. Choi, J. Kim, Improved photo-and chemical-responses of graphene via porphyrin-functionalization for flexible, transparent, and sensitive sensors, Nanotechnology 30(21) (2019) 215501.

[11] S.A.L. Rousseaux, J.Q. Gong, R. Haver, B. Odell, T.D.W. Claridge, L.M. Herz, H.L. Anderson, Self-assembly of russian doll concentric porphyrin nanorings, J. Am. Chem. Soc. 137(39) (2015) 12713-12718.

[12] Philip M. Punt, G.H. Clever, Imidazole-modified G-quadruplex DNA as metal-triggered peroxidase, Chem. Sci. 10(8) (2019) 2513-2518.

[13] L.A. Solomon, J.B. Kronenberg, H.C. Fry, Control of heme coordination and catalytic activity by conformational changes in peptide-amphiphile assemblies, J. Am.

Chem. Soc. 139(25) (2017) 8497-8507.

[14] C.B. Liu, H.C. Zhao, P.M. Hou, B. Qian, X. Wang, C.Y. Guo, L.P. Wang, Efficient graphene/cyclodextrin-based nanocontainer: synthesis and host-guest inclusion for self-healing anticorrosion application, ACS Appl. Mat. Inter. 10(42) (2018) 36229-36239.

[15] Y.T. Shi, H.P. Li, J. Cheng, T.T. Luan, D. Liu, Y.F. Cao, X.D. Zhang, H. Wei, Y.L. Liu, G.H. Zhao, Entirely oligosaccharide-based supramolecular amphiphiles constructed via host-guest interactions as efficient drug delivery platforms, Chem. Commun. 53(91) (2017) 12302-12305.

[16] H.B. Jin, L. Yang, M.J.R. Ahonen, M.H. Schoenfisch, Nitric oxide-releasing cyclodextrins, J. Am. Chem. Soc. 140(43) (2018) 14178-14184.

[17] Y. Xu, M.Y. Cui, P.A. Patsis, M. Günther, X.G. Yang, K. Eckert, Y.X. Zhang, Reversibly assembled electroconductive hydrogel via a host-guest interaction for 3D cell culture, ACS Appl. Mat. Inter. 11(8) (2019) 7715-7724.

[18] C. Falaise, M.A. Moussawi, S. Floquet, P.A. Abramov, M.N. Sokolov, M. Haouas, E. Cadot, Probing dynamic library of metal-oxo building blocks with γ-cyclodextrin, J. Am. Chem. Soc. 140(36) (2018) 11198-11201.

[19] X.Q. Wei, W.H. Wu, R. Matsushita, Z.Q. Yan, D.Y. Zhou, J.J. Chruma, M. Nishijima, G. Fukuhara, T. Mori, Y. Inoue, C. Yang, Supramolecular photochirogenesis driven by higher-order complexation: Enantiodifferentiating photocyclodimerization of 2-anthracenecarboxylate to slipped cyclodimers via a 2:2 complex with β-cyclodextrin, J. Am. Chem. Soc. 140(11) (2018) 3959-3974.

[20] T. Ueda, S. Kumeda, H. Kitagishi, K. Kano, Intramolecular oxidative O-demethylation in a per-O-methylated β-cyclodextrin-iron porphyrin inclusion complex in aqueous solution, Chem. Lett. 42(11) (2013) 1366-1368.

[21] K. Kano, H. Kitagishi, C. Dagallier, M. Kodera, T. Matsuo, T. Hayashi, Y. Hisaeda, S. Hirota, Iron porphyrin-cyclodextrin supramolecular complex as a functional model of myoglobin in aqueous solution, Inorg. Chem. 45(11) (2006) 4448-4460.

[22] H. Kitagishi, Y. Sugaya, K. Komazawa, M. Tamaki, K. Kano, Participation of hydroxyl radical in the formation of verdoheme-type compound in the reaction of a ferric porphyrin with hydrogen peroxide, Chem. Lett. 46(4) (2017) 509-512.

[23] Q.W. Zhang, J.A.A.W. Elemans, P.B. White, R.J.M. Nolte, A manganese porphyrin-α-cyclodextrin conjugate as an artificial enzyme for the catalytic epoxidation of polybutadiene, Chem. Commun. 54(44) (2018) 5586-5589.

[24] M. Morisue, T. Yumura, R. Sawada, M. Naito, Y. Kuroda, Y. Chujo, Oligoamylose-entwined porphyrin: excited-state induced-fit for chirality induction, Chem. Commun. 52(12) (2016) 2481-2484.

[25] S. Minegishi, A. Yumura, H. Miyoshi, S. Negi, S. Taketani, R. Motterlini, R. Foresti, K. Kano, H. Kitagishi, Detection and removal of endogenous carbon mnoxide by selective and cell-permeable hemoprotein model complexes, J. Am. Chem. Soc. 139(16) (2017) 5984-5991.

[26] Z.Y. Tian, L.L. Si, K. Meng, X.S. Zhou, Y.M. Zhang, D.M. Zhou, S.L. Xiao, Inhibition of influenza virus infection by multivalent pentacyclic

triterpene-functionalized per-O-methylated cyclodextrin conjugates, Eur. J. Med. Chem. 134 (2017) 133-139.

[27] Y. Chen, P.X. Yuan, A.J. Wang, X.L. Luo, Y.D. Xue, L. Zhang, J.J. Feng, A novel electrochemical immunosensor for highly sensitive detection of prostate-specific antigen using 3D open-structured PtCu nanoframes for signal amplification, Biosens. Bioelectron. 126 (2019) 187-192.

[28] H. Cheema, A. Baumann, E.K. Loya, P. Brogdon, L.E. McNamara, C.A. Carpenter, N.I. Hammer, S. Mathew, C. Risko, J.H. Delcamp, Near-infrared-absorbing indolizine-porphyrin push-pull dye for dye-sensitized solar cells, ACS Appl. Mat. Inter. 11(18) (2019) 16474-16489.

[29] D. Basu, S. Mazumder, J. Niklas, H. Baydoun, D. Wanniarachchi, X. Shi, R.J. Staples, O. Poluektov, H.B. Schlegel, C.N. Verani, Evaluation of the coordination preferences and catalytic pathways of heteroaxial cobalt oximes towards hydrogen generation, Chem Sci 7(5) (2016) 3264-3278.

[30] S. Ikejiri, Y. Takashima, M. Osaki, H. Yamaguchi, A. Harada, Solvent-free photoresponsive artificial muscles rapidly driven by molecular machines, J. Am. Chem. Soc. 140(49) (2018) 17308-17315.

[31] S.L. Xiao, M. Yang, F. Yu, L.H. Zhang, D.M. Zhou, P. Sinaÿ, Y.M. Zhang, Synthesis of four mono-functionalized α-cyclodextrin derivatives for further confirming DIBAL-H-promoted bis-de-O-methylation mechanism, Tetrahedron 69(20) (2013) 4053-4060.

[32] Y. Chen, X.X. Zheng, X.Y. Huang, A.J. Wang, Q.L. Zhang, H. Huang, J.J. Feng,

Trimetallic PtRhCo petal-assembled alloyed nanoflowers as efficient and stable bifunctional electrocatalyst for ethylene glycol oxidation and hydrogen evolution reactions, J. Colloid Interface Sci. 559 (2020) 206-214.

[33] J.J. Duan, X.X. Zheng, H.J. Niu, J.J. Feng, Q.L. Zhang, H. Huang, A.J. Wang, Porous dendritic PtRuPd nanospheres with enhanced catalytic activity and durability for ethylene glycol oxidation and oxygen reduction reactions, J. Colloid Interface Sci. (2019) https://doi.org/10.1016/j.jcis.2019.10.082.

[34] K. Kano, Y. Itoh, H. Kitagishi, T. Hayashi, S. Hirota, A supramolecular receptor of diatomic molecules (O_2, CO, NO) in aqueous solution, J. Am. Chem. Soc. 130(25) (2008) 8006-8015.

[35] K. Zhu, Q. Luo, S.Z. Kang, L.X. Qin, G.D. Li, X.Q. Li, The study of a novel cobalt-implanted pyridylporphyrin/graphene oxide nanohybrid for enhanced photocatalytic hydrogen evolution and its electron transfer mechanism, Nanoscale 10(39) (2018) 18635-18641.

[36] P. Antal, B. Drahoš, R. Herchel, Z. Trávníček, Late First-Row Transition-Metal Complexes Containing a 2-Pyridylmethyl Pendant-Armed 15-Membered Macrocyclic Ligand. Field-Induced Slow Magnetic Relaxation in a Seven-Coordinate Cobalt(II) Compound, Inorg. Chem. 55(12) (2016) 5957-5972.

[37] A.K. Mondal, A. Mondal, B. Dey, S. Konar, Influence of the Coordination Environment on Easy-Plane Magnetic Anisotropy of Pentagonal Bipyramidal Cobalt(II) Complexes, Inorg. Chem. 57(16) (2018) 9999-10008.

[38] B.Q. Li, C.X. Zhao, S.M. Chen, J.N. Liu, X. Chen, L. Song, Q. Zhang,

Framework-porphyrin-derived single-atom bifunctional oxygen electrocatalysts and their applications in Zn-air batteries, Adv. Mater. 0(0) (2019) 1900592.

[39] L.Q. Jiang, L.L. Cui, X.Q. He, Cobalt-porphyrin noncovalently functionalized graphene as nonprecious-metal electrocatalyst for oxygen reduction reaction in an alkaline medium, J. Solid State Electrochem. 19(2) (2015) 497-506.

[40] G.J. Liu, H.P. Bai, B. Zhang, H. Peng, Role of organic components in electrocatalysis for renewable energy storage, Chem. Eur. J. 24(69) (2018) 18271-18292.

[41] Z. Li, L. Wei, W.-J. Jiang, Z. Hu, H. Luo, W. Zhao, T. Xu, W. Wu, M. Wu, J.-S. Hu, Chemical state of surrounding iron species affects the activity of Fe-Nx for electrocatalytic oxygen reduction, Appl. Catal. B Environ. 251 (2019) 240-246.

[42] S. Banerjee, Y. Nabae, Ferric porphyrin–based polymers for electrochemical oxygen reduction, Catal. Today 332 (2019) 109-114.

[43] Y.Y. Zhang, A.M. Wang, S.Y. Ren, Z.J. Wen, X.J. Tian, D.S. Li, J.Y. Li, Effect of surface properties of activated carbon fiber cathode on mineralization of antibiotic cefalexin by electro-fenton and photoelectro-fenton treatments: Mineralization, kinetics and oxidation products, Chemosphere 221 (2019) 423-432.

[44] M.R. Abdul Hamid, S. Park, J.S. Kim, Y.M. Lee, H.-K. Jeong, In situ formation of zeolitic-imidazolate framework thin films and composites using modified polymer substrates, J. Mater. Chem. A 7(16) (2019) 9680-9689.

[45] T. Liang, X. Guo, J. Wang, Y. Wei, D. Zhang, S. Kong, Green synthesis of porous graphene-like nanosheets for high-sensitivity nonenzymatic hydrogen peroxide

biosensor, Mater. Lett. 254 (2019) 28-32.

[46] M. Preethika, A.K. Sundramoorthy, Humic acid/halloysite nanotube/flavin adenine dinucleotide nanocomposite based selective electrochemical biosensor for hydrogen peroxide, Appl. Surf. Sci. 488 (2019) 503-511.

[47] M. Hamtak, M. Hosseini, L. Fotouhi, M. Aghazadeh, A new electrochemiluminescence biosensor for the detection of glucose based on polypyrrole/polyluminol/Ni$(OH)_2$–C_3N_4/glucose oxidase-modified graphite electrode, Anal. Methods 10(47) (2018) 5723-5730.

[48] M.Y. Shi, M. Xu, Z.Y. Gu, Copper-based two-dimensional metal-organic framework nanosheets as horseradish peroxidase mimics for glucose fluorescence sensing, Anal Chim Acta 1079 (2019) 164-170.

Captions

Scheme 1. The scheme of the synthesis of Co^{III}-PPIX@Py2CD and its application for H_2O_2 detection

Fig. 1. (A) The CD absorption spectra of Co^{III}-PPIX (curve a), Py2CD (curve b), and Co^{III}-PPIX@Py2CD (curve c). (B) The UV-vis absorption spectra of Co^{III}-PPIX (curve a) and Co^{III}-PPIX@Py2CD (curve b).

Fig. 2. (A) The ^1H NMR spectrum of Py2CD in the PBS under 25 °C. (B) The high-resolution N 1s XPS spectra of Py2CD (curve a) and Co^{III}-PPIX@Py2CD (curve b). (C) The high-resolution Co 2p XPS spectra of Co^{III}-PPIX (curve a) and Co^{III}-PPIX@Py2CD (curve b).

Fig. 3. (A) The CV curves of Co^{III}-PPIX (curve a), Co^{III}-PPIX@Py2CD (curve b) and Co^{III}-PPIX@Py2CD with 10 mM H_2O_2 (curve c) in the air-saturated PBS. (B) The CV curves of Co^{III}-PPIX (curve a) and Co^{III}-PPIX@Py2CD (curve b) in the N_2-saturated PBS. Inset in Fig. 3B display the plots of the scan rate *vs.* i_{pc} of Co^{III}-PPIX (line a1) and Co^{III}-PPIX@Py2CD (line b1). (C) The CV curves of Co^{III}-PPIX@Py2CD in the pH range of 5~9. Inset in Fig. 3C is the peak potential (E_p) *vs* pH.

Fig. 4. (A) Chronoamperometric responses of Co^{III}-PPIX@Py2CD by successive

addition of H_2O_2 at the applied potential of -0.30 V in the electrolyte. Inset in Fig. 4A is the local zoom of the i~t curve. (B) The calibration curve of the reduction current against the H_2O_2 concentration. The amperometric responses in the presence of (C) reductive (DA and AA) and (D) oxidative (Fe^{3+}, $S_2O_8^{2-}$, and MnO_4^-) interferences.

Figures

Scheme 1.

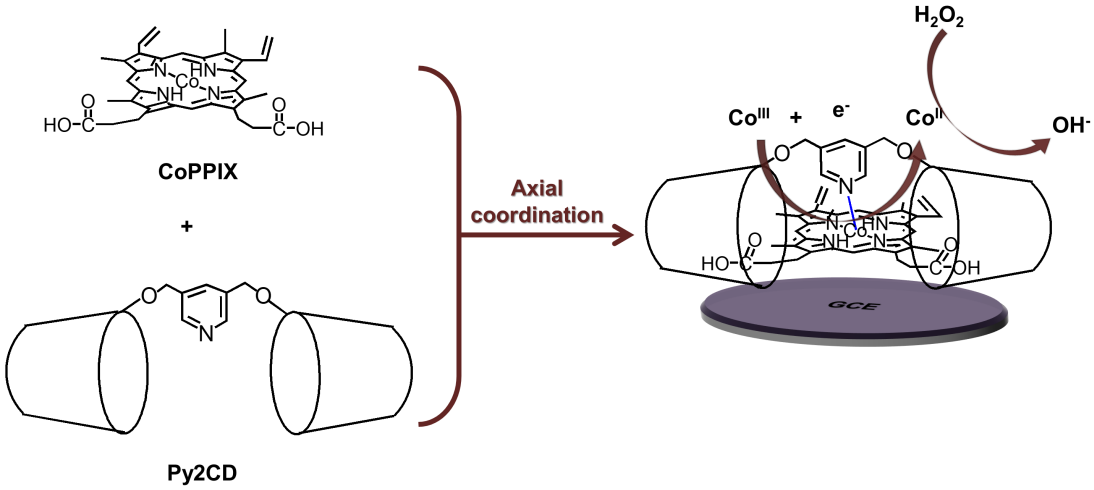

Fig. 1

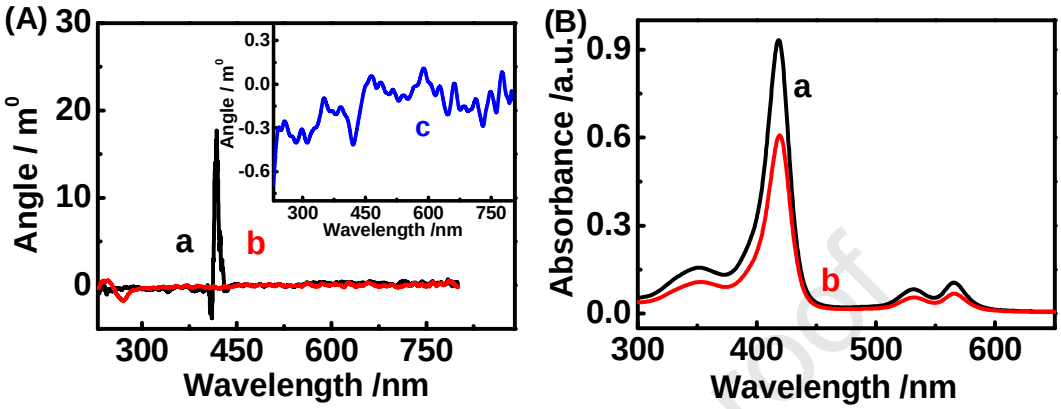

Fig. 2

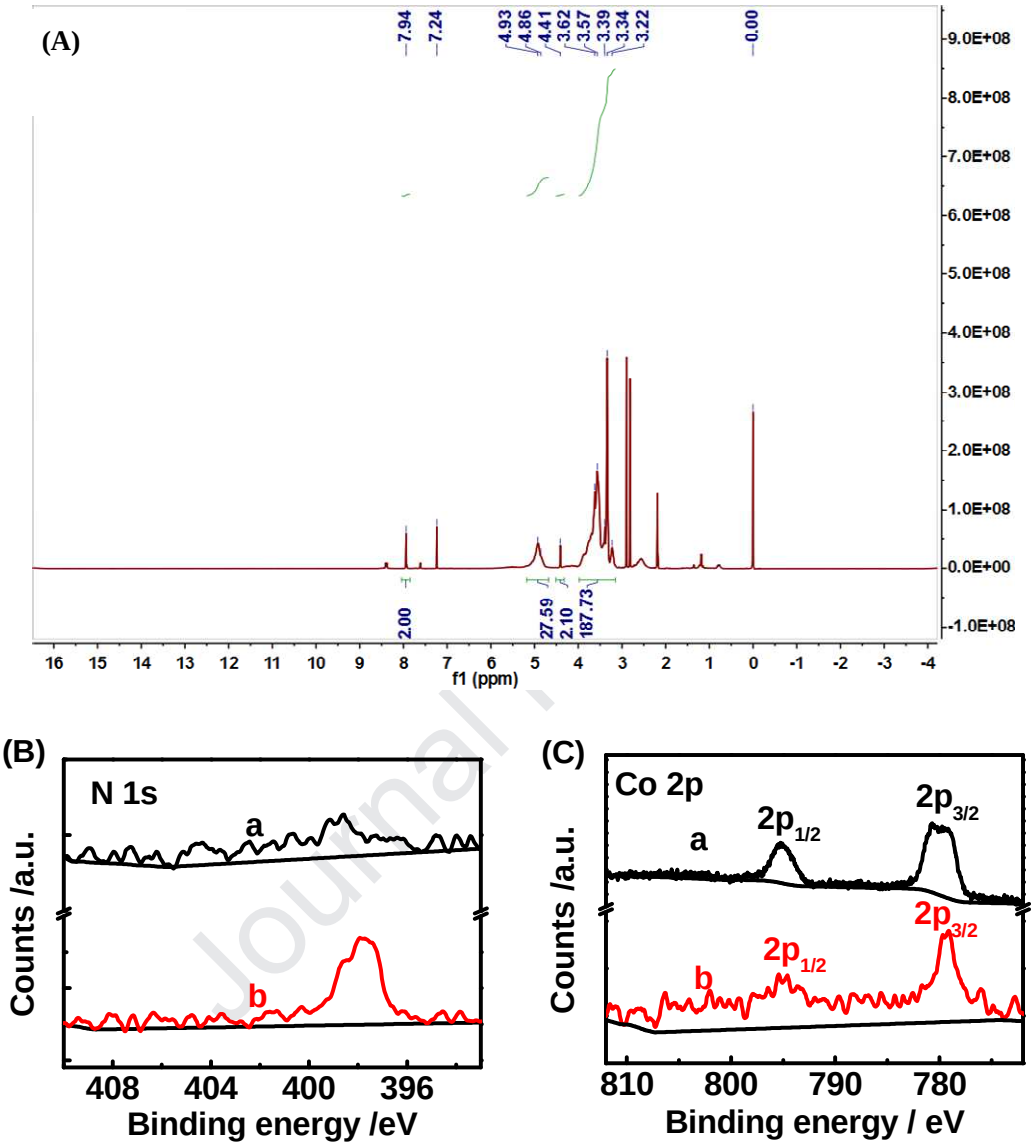
(A)
7.94
7.24
4.93
4.86
4.41
3.62
3.57
3.39
3.34
3.22
0.00
2.00
27.59
2.10
187.73
f1 (ppm)
(B)
N 1s
a
b
Counts /a.u.
Binding energy /eV
(C)
Co 2p
a
2p1/2
2p3/2
b
Counts /a.u.
Binding energy / eV

Fig. 3

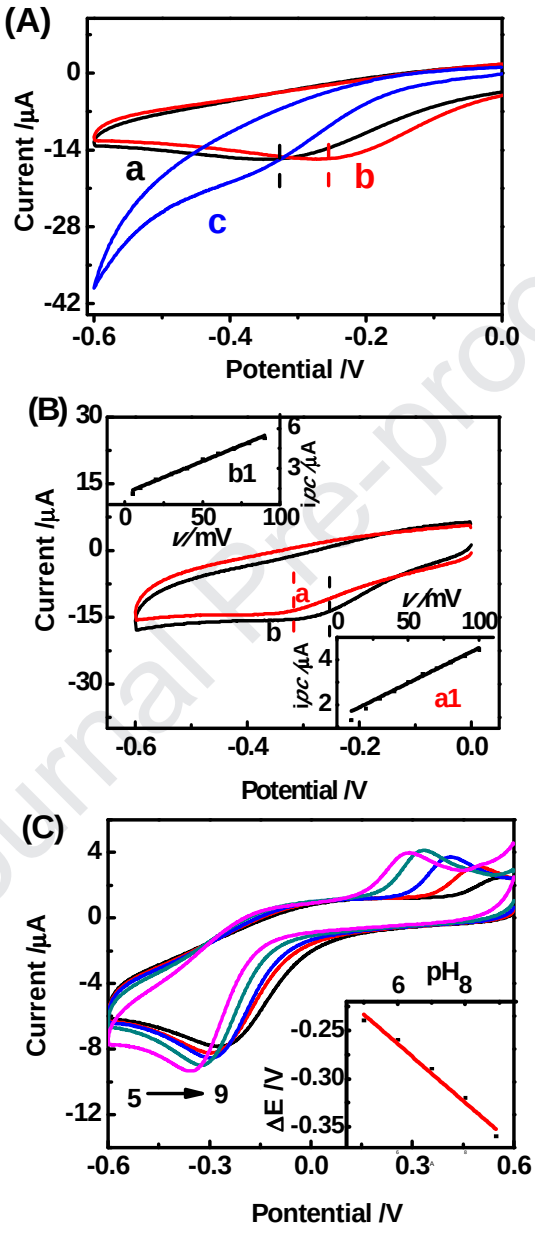

Fig. 4

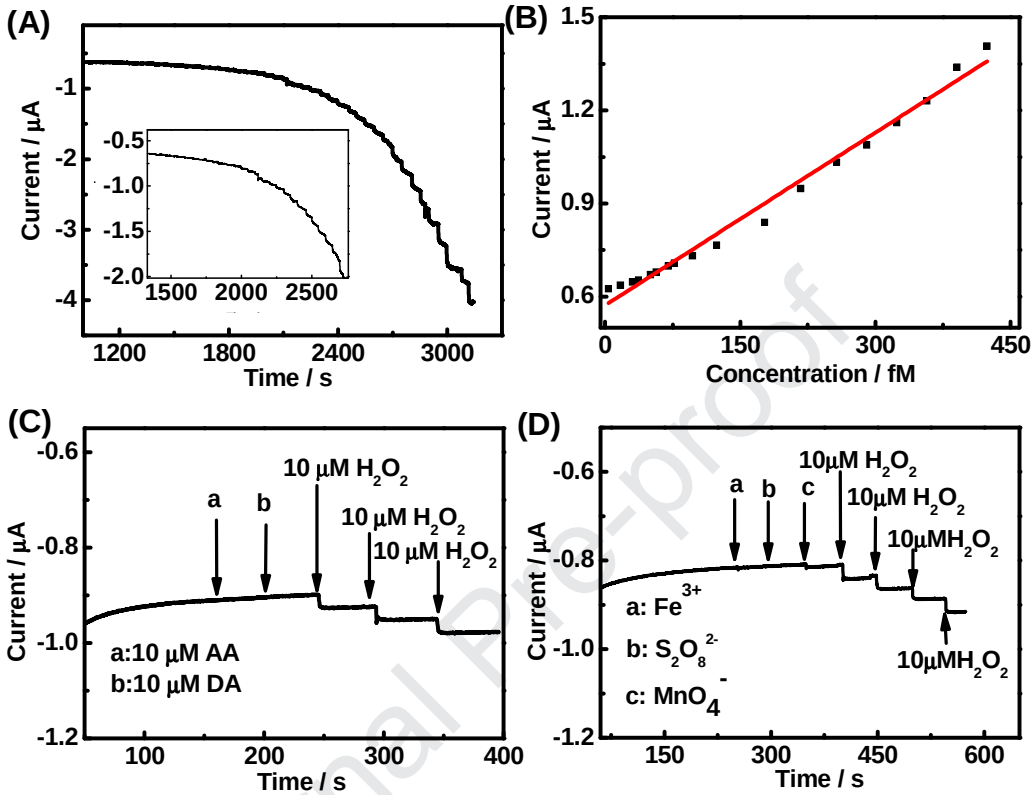

Table 1. Comparison of the analytical data of the as-fabricated biosensor for the determination of H_2O_2 with those reported previously.

Analytical methods	Linear ranges	Detection limits	References
Electrochemisty	0.2-19 mM	2.75 mM	[44, 45]
Electrochemisty	1-250 mM	0.49 mM	[46]
ECL	0.5-500 mM	0.04 mM	[47]
Fluorescence	10-100 mM	0.41 mM	[48]
Electrochemisty	1 μM -10 mM	0.25 mM	This work

Research Highlights

- ► Py2CD was obtained by the covalent linkage of two β-CDs monomers with 3,5-bis (bromomethyl) pyridine.
- ► The Co^{III}-PPIX@Py2CD were prepared by acyl chlorination reaction between the Co^{III} of Co^{III}-PPIX and pyridine N of Py2CD.
- ► The catalyst dramatically improved the electronic conductivity and amplified the catalytic signals towards H_2O_2 reduction.
- ► An ultrasensitive chronoamperometric sensor was developed for H_2O_2 detection.

Declaration of interests

☒ ✓ The authors declare that they have no known competing financial interests or personal relationships that could have appeared to influence the work reported in this paper.

☐The authors declare the following financial interests/personal relationships which may be considered as potential competing interests:

The authors declare no competing financial interest.